AMERICAN SOCIETY FOR MICROBIOLOGY | Applied and Environmental Microbiology®

ENVIRONMENTAL MICROBIOLOGY

Multi-omic Analyses of Extensively Decayed *Pinus contorta* Reveal Expression of a Diverse Array of Lignocellulose-Degrading Enzymes

Chiaki Hori,[a] Jill Gaskell,[b] Dan Cullen,[b] Grzegorz Sabat,[c] Philip E. Stewart,[d] Kathleen Lail,[e] Yi Peng,[e] Kerrie Barry,[e] Igor V. Grigoriev,[e,f] Annegret Kohler,[g] Laure Fauchery,[g] Francis Martin,[g] Carolyn A. Zeiner,[h] Jennifer M. Bhatnagar[h]

[a]School of Engineering, Hokkaido University, Sapporo, Japan
[b]USDA, Forest Products Laboratory, Madison, Wisconsin, USA
[c]University of Wisconsin-Madison Biotechnology Center, Madison, Wisconsin, USA
[d]Rocky Mountain Laboratories, NIAID, NIH, Hamilton, Montana, USA
[e]US Department of Energy Joint Genome Institute, Walnut Creek, California, USA
[f]Department of Plant and Microbial Biology, University of California Berkeley, Berkeley, California, USA
[g]Institut National de la Recherche Agronomique, Unité Mixte de Recherche 1136, Institut National de la Recherche Agronomique-Université de Lorraine, Interactions Arbres/Micro-organismes, Champenoux, France
[h]Department of Biology, Boston University, Boston, Massachusetts, USA

ABSTRACT Fungi play a key role cycling nutrients in forest ecosystems, but the mechanisms remain uncertain. To clarify the enzymatic processes involved in wood decomposition, the metatranscriptomics and metaproteomics of extensively decayed lodgepole pine were examined by RNA sequencing (RNA-seq) and liquid chromatography-tandem mass spectrometry (LC-MS/MS), respectively. Following *de novo* metatranscriptome assembly, 52,011 contigs were searched for functional domains and homology to database entries. Contigs similar to basidiomycete transcripts dominated, and many of these were most closely related to ligninolytic white rot fungi or cellulolytic brown rot fungi. A diverse array of carbohydrate-active enzymes (CAZymes) representing a total of 132 families or subfamilies were identified. Among these were 672 glycoside hydrolases, including highly expressed cellulases or hemicellulases. The CAZymes also included 162 predicted redox enzymes classified within auxiliary activity (AA) families. Eighteen of these were manganese peroxidases, which are key components of ligninolytic white rot fungi. The expression of other redox enzymes supported the working of hydroquinone reduction cycles capable of generating reactive hydroxyl radicals. These have been implicated as diffusible oxidants responsible for cellulose depolymerization by brown rot fungi. Thus, enzyme diversity and the coexistence of brown and white rot fungi suggest complex interactions of fungal species and degradative strategies during the decay of lodgepole pine.

IMPORTANCE The deconstruction of recalcitrant woody substrates is a central component of carbon cycling and forest health. Laboratory investigations have contributed substantially toward understanding the mechanisms employed by model wood decay fungi, but few studies have examined the physiological processes in natural environments. Herein, we identify the functional genes present in field samples of extensively decayed lodgepole pine (*Pinus contorta*), a major species distributed throughout the North American Rocky Mountains. The classified transcripts and proteins revealed a diverse array of oxidative and hydrolytic enzymes involved in the degradation of lignocellulose. The evidence also strongly supports simultaneous attack by fungal species employing different enzymatic strategies.

KEYWORDS *Pinus*, brown rot, metaproteome, metatranscriptome, white rot

Received 15 May 2018 **Accepted** 4 August 2018

Accepted manuscript posted online 10 August 2018

Citation Hori C, Gaskell J, Cullen D, Sabat G, Stewart PE, Lail K, Peng Y, Barry K, Grigoriev IV, Kohler A, Fauchery L, Martin F, Zeiner CA, Bhatnagar JM. 2018. Multi-omic analyses of extensively decayed *Pinus contorta* reveal expression of a diverse array of lignocellulose-degrading enzymes. Appl Environ Microbiol 84:e01133-18. https://doi.org/10.1128/AEM.01133-18.

Editor Hideaki Nojiri, University of Tokyo

Address correspondence to Dan Cullen, dcullen@wisc.edu.

Fungi play a critical role in recycling of forest carbon via wood decomposition. Significant effort has focused on describing the microbial communities using conventional plating techniques, observations of conspicuous fungal fruiting bodies (1), enzyme assays (2), and metagenomics analyses of rRNA and other conserved genes (3–5). The complexity and interactions among physiologically active wood decay microbes remain poorly understood, although recent work on forest soils and litter may be relevant, at least in terms of experimental tools (6–11).

Two forms of wood decay are generally recognized (12, 13). Brown rot fungi rapidly depolymerize cellulose via oxidative systems. Bulk lignin is left behind as a polymeric residue. In contrast, white rot fungi degrade and metabolize lignin, while cellulose is hydrolyzed by conventional carbohydrate-active enzymes (CAZymes) (14). Except for rare cases (15), genome annotation supports these classifications; white rot fungi feature genes encoding ligninolytic peroxidases and numerous cellulases, while brown rot fungi have few, if any, of these genes (16). Efficient degradation and mineralization of native lignin are accomplished almost exclusively by white rot basidiomycetes, some of which are closely related to brown rot fungi. The efficiency by which these fungi degrade cellulose and lignin has generated considerable interest in bioprocess development.

Toward the identification of enzymes directly involved in the natural decomposition of wood, metatranscriptome and metaproteome investigations were performed on decayed lodgepole pine (*Pinus contorta*), a fire-adapted species widely distributed throughout the North American Rocky Mountains.

RESULTS

Metatranscriptome. Analyses were focused on poly(A) RNA purified from extensively decayed lodgepole pine samples collected in western Montana national forests. To provide a broad perspective, sampling included distinct locations and fire histories. Avoiding direct contact with soil/litter, the loose material was collected from the logs' upper surface. A total of 2.9×10^8 Illumina RNA sequencing (RNA-seq) reads were generated from the amplified poly(A) RNA. *De novo* assembly yielded 274,233 contigs, each with a minimum of 100 reads. To add confidence to BLASTx queries, these were further filtered to 52,011 contigs over 750 bp in length (Table 1).

BLASTx searches of metatranscriptome contigs against NCBI RefSeq, GO, InterPro, and EC databases supported putative classifications and revealed conserved protein domains directly supporting function and/or features potentially involved (e.g., secretion signals and transmembrane helices) (Table 1). Using a conservative E value threshold (10^{-15}), 41% of the contigs were related only to hypothetical proteins or were otherwise unassigned (Fig. 1). A total of 1,316 putative CAZyme-encoding transcripts were identified. Impressive numbers of transporters (1,631) and cytochrome P450s (203) were also found, and although their precise functions are difficult to predict, some are likely to play an important role in the uptake and metabolism of low-molecular-weight products during cell wall degradation. A substantial number of extracellular proteases together with oligopeptide and amino acid transporters (see Data Set S1 in the supplemental material) are probably indicative of nitrogen scavenging within the N-limited substrate. Not surprisingly, approximately 50% of the RefSeq hits were encoding intracellular structural proteins (e.g., actin) or enzymes involved in protein synthesis (e.g., ribosomal proteins) and central metabolism (e.g., glyceraldehyde-3-phosphate dehydrogenase). Without doubt, relaxing the BLAST thresholds and/or including contigs $<$750 bp would identify additional sequences, possibly including those encoding small secreted proteins (17). A detailed description of contigs is presented in Data Set S1.

Of the 1,316 CAZymes, 162 CAZymes were classified as members of an auxiliary activity (AA) family (Fig. 2) (18). Clearly demonstrating white rot ligninolysis, eight contigs encoding manganese-dependent lignin peroxidases (MnPs) were among the 30 most highly expressed AA-encoding genes (Table 2). Abundant transcripts corresponding to eight alcohol oxidases were also identified, and all were closely related to

TABLE 1 Metatranscriptome and metaproteome summary

Parameter[a]	No.
RNA-seq reads	291,596,160
Contigs >100 reads	274,233
Avg length (bp)	590
Contigs >100 reads, >750 bp	52,011
IPR domains	42,307
GO assignments	33,523
GO after merging	116,997
Confirmed IPS GOs	103,837
EC assignments	7,901
Oxidoreductases	2,083
Transferases	1,553
Hydrolases	3,242
Lyases	556
Isomerases	389
Ligases	281
TMHs predicted	10,510
Eukaryotic secretion signal	2,705
Protein detected[b]	1,935

[a]IPR, InterPro; GO, Gene Ontology; IPS, InterPro Scan; TMHs, transmembrane head proteins.

Gloeophyllum trabeum methanol oxidase (19). Two benzoquinone reductases may participate in a redox cycle tied to hydroxyl radical generation during brown rot decay (20–22). Surprisingly, the highest transcript levels among AA-encoding genes were attributed to lytic polysaccharide monooxygenases (LPMO; Table 2). Previously classified as glycoside hydrolase 61 (GH61), these copper-dependent enzymes have been shown to cleave C-1 or C-4 glycosidic bonds (reviewed in reference 23).

Beyond the AA families, 1,154 additional CAZymes were identified, including 672 glycoside hydrolases (GHs), 154 glycosyltransferases (GTs), 105 carbohydrate esterases (CEs), 13 polysaccharide lyases (PLs), and 210 carbohydrate binding modules. Glycoside hydrolase families associated with cellulose degradation, e.g., GH5_5, GH6, GH7, GH12, and GH45, were particularly abundant (Fig. 3 and Table 3). Total transcripts classified as the "exo"-acting cellobiohydrolases (GH7s and GH6s) were substantially increased due to the activity of relatively few, but highly expressed, genes (Fig. 3). Similarly, of 25 GH5_5 contigs, 4921502_1 and 1142146_1 (Table 3) disproportionately contributed 45% of the total reads (Fig. 3; see also Data Set S1 in the supplemental material). The GH7, GH6, and GH5_5 families accounted for 25%, 15%, and 15% of the cellulase reads, respectively.

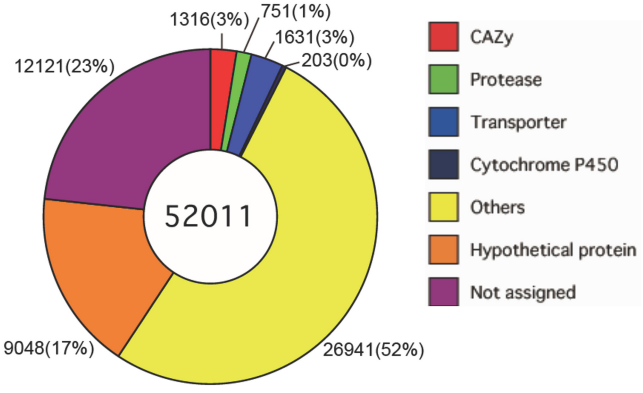

FIG 1 Distribution of 52,011 contigs. Hypotheticals includes conserved hypothetical, predicted proteins, and uncharacterized proteins. Transporters include permeases and those assigned to the major facilitator superfamily (MFS).

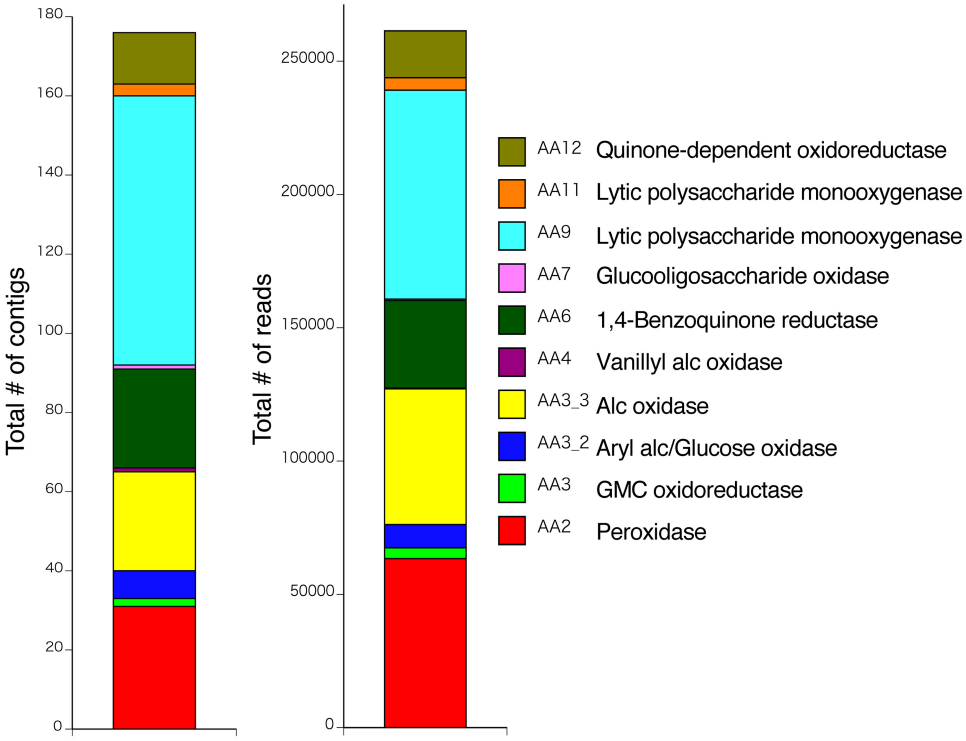

FIG 2 Number of contigs and reads assigned to AA families. GMC, glucose-methanol-choline; Alc, alcohol.

Enzymes broadly characterized as hemicellulases were among the most highly expressed transcripts and included GH114 endo-α-1-4-polygalactosaminidase (3859657_1), GH10 endo-1,4-β xylanase (3561636_2), GH53 endo-1,4-β-galactanase, and a GH27 α-galactosidase (910111_1) (Table 3). The numbers of contigs and total reads assigned to potential hemicellulase families are shown in Fig. 4. Several of these are involved in the degradation of galactoglucomannan, arabinoglucuronoxylan, and arabinogalactan, all of which are components of softwood hemicellulose. The complete breakdown of these substrates may involve the combined activities of multiple GH families. For example, β-mannanases belonging to GH2, GH5_7, and GH5_41 represented 15% of the hemicellulose-assigned reads (Data Set S1). In addition to plant cell wall degradation, β-1,3-glucans and chitin from insects and fungal cell walls are likely substrates for GHs, such as GH18 chitinases. Beyond these hydrolases, CEs associated with the removal of an acetyl substitution from hemicellulose and chitin (CE1, CE4, and CE16) were major components of the transcriptome (Data Set S1).

Contigs with putative functions were most frequently related to basidiomycetes (Fig. 5; see also Fig. S3 and Data Set S1 in the supplemental material), although sequences closely related to other eukaryotes, or their viruses, were also detected. Of the 52,011 contigs, 39,765 contigs gave significant BLASTx score E values ($<10^{-15}$) to the NCBI RefSeq database. Translations of these contigs, plus the extended open reading frames (ORFs) of those contigs without significant BLASTx scores, were queried against the NCBI nonredundant (NR) protein database. A total of 39,973 proteins gave significant hits (E values $< 10^{-15}$), and these were distributed among 2,810 species, including 1,387 species with a single hit. Forty-two species accounted for approximately 50% of the top BLASTp hits (Fig. 5, left). This overall pattern of similarity to basidiomycete genes was also observed for a much smaller subset of 1,316 CAZyme-encoding genes (Fig. 5, right). The skewed representation toward basidiomycetes is also evident when considering up to 10 database entries most closely related to each contig (Fig. S3).

Many genes involved in lignocellulose deconstruction were highly expressed, including the above-mentioned exo- and endo-acting cellulases, transporters, and oxi-

TABLE 2 Contigs predicted to encode proteins with auxiliary activities ordered by sequence reads[a]

Contig	No. of reads	Length (bp)	CAZy family[b]	Putative function	E value[c]	Similarity mean (%)[d]	Comment[e]
5367253_3	10,056	1,225	AA3_3	Methanol oxidase	0	93.1	MS
2929739_1	9,675	873	AA9	LPMO	3.35E−54	57.9	SS
1507360_1	9,562	1,007	AA6	Benzoquinone reductase	5.87E−86	75.1	MS
4793784_4	8,517	892	AA2	Manganese peroxidase	7.12E−98	73.5	
3105967_1	8,470	824	AA9	LPMO	6.42E−95	70.8	SS
1303515_1	7,776	1,316	AA2	Manganese peroxidase	1.91E−158	76	
798557_1	7,736	1,563	AA3_3	Alcohol oxidase	0	90.8	MS
4253668_1	7,400	862	AA9	LPMO	4.27E−113	76.1	SS
1203164_1	6,279	820	AA9	LPMO	1.78E−72	84.1	CBM1
694467_2	5,891	1,568	AA9	LPMO	5.19E−68	72.2	
3968694_1	5,536	1,140	AA2	Manganese peroxidase	2.44E−114	77.9	
3834150_1	5,521	862	AA6	Benzoquinone reductase	5.01E−103	82.9	MS
3968694_2	5,211	1,057	AA2	Manganese peroxidase	1.94E−80	76.4	
3406352_1	4,719	1,151	AA2	Manganese peroxidase	1.00E−128	75	
536886_1	4,574	1,455	AA3_3	Alcohol oxidase	0	93.8	MS
5221162_1	4,332	865	AA9	LPMO	4.28E−36	65.7	
4793784_3	4,023	932	AA2	Manganese peroxidase	7.40E−106	72.2	MS
1201987_1	3,747	1,074	AA9	LPMO	5.11E−116	83.2	SS
2929739_3	3,640	915	AA9	LPMO	1.91E−47	60.4	SS, MS
2280897_3	3,374	1,119	AA3_3	Alcohol oxidase	0	92.8	MS
4793784_1	3,310	901	AA2	Manganese peroxidase	3.24E−92	71.3	MS
4582340_1	3,263	929	AA9	LPMO	2.36E−83	82	CBM1
2280897_7	3,087	1,095	AA3_3	Alcohol oxidase	8.37E−148	92	MS
798557_5	3,018	1,095	AA3_3	Alcohol oxidase	0	87.6	MS
1303515_3	2,984	1,055	AA2	Manganese peroxidase	1.35E−119	80.1	
2353562_1	2,843	1,263	AA3	GMC oxidoreductase	3.97E−59	50.4	
3751681_1	2,838	912	AA9	LPMO	2.47E−100	79.7	SS
798557_17	2,693	1,051	AA3_3	Alcohol oxidase	9.20E−171	89	MS
4109481_1	2,461	1,271	AA3_2	GMC oxidoreductase	1.38E−111	65.3	
1227884_4	2,455	1,033	AA3_3	Alcohol oxidase	1.06E−175	91	MS

[a]Complete information, including BLASTx analyses, InterPro, and Gene Ontology designations, as well as mass spectrometry results, are listed in Data Set S1 in the supplemental material.
[b]CAZy families were identified by dbCAN (Yin et al. [56]).
[c]E value of top BLASTx hit.
[d]Average sequence similarity to the top 10 BLASTx hits.
[e]SS, SignalP-determined secretion signal; MS, LC-MS/MS-identified proteins; CBM1, carbohydrate-binding module family 1.

doreductases (Tables 2 and 3; see also Table S1 in the supplemental material). In some instances, possible prokaryote sequences were detected. For example, the predicted amino acid sequence of 1384861_1, a putative cellobiohydrolase (Table 3), was 43% (E value 10^{-102}) identical to that of *Sorangium cellulosum* (GenBank accession no. KYG02679). However, the contig sequence is also similar to those with various fungal accession numbers, such as OAL51409 from *Pyrenochaeta* sp., but polyadenylation is absent, as expected if originating from prokaryotic organisms. Evidence supporting the prokaryotic origins of other highly expressed genes is more compelling. Specifically, contigs 94066_1, 4739131_4, and 2374420_1 are among the 30 most highly expressed glycoside hydrolases (Table 3) and most closely related to those of *Kutzneria* sp. (RefSeq accession no. WP_084578858), *Enhygromyxa salina* (NCBI accession no. KIG15205), and *Actinobacteria* bacterium (NCBI accession no. OLB81315) genes, respectively (Data Set S1). All have short 3′-poly(A) tracts of 16 to 24 residues and, in each case, the 10 most closely related database entries are also derived from bacteria.

A total of 28 contigs were most closely related to cDNAs derived from an "uncultured eukaryote" in *Picea abies* forest soils (7). Twenty-two of these encode putative CAZy domains (Data Set S1). The deduced amino acid sequence of a highly expressed GH45-encoding gene (4034495_1; Table 3) is 76% identical to that with NCBI accession no. CCA94939 (7).

Metaproteome. Tandem mass spectrometry (MS/MS) data matched 1,964 proteins corresponding to 1,935 contigs. Of these mass spectrometry-identified proteins, the majority were encoded by orthologous sets of housekeeping genes, such as 40S and

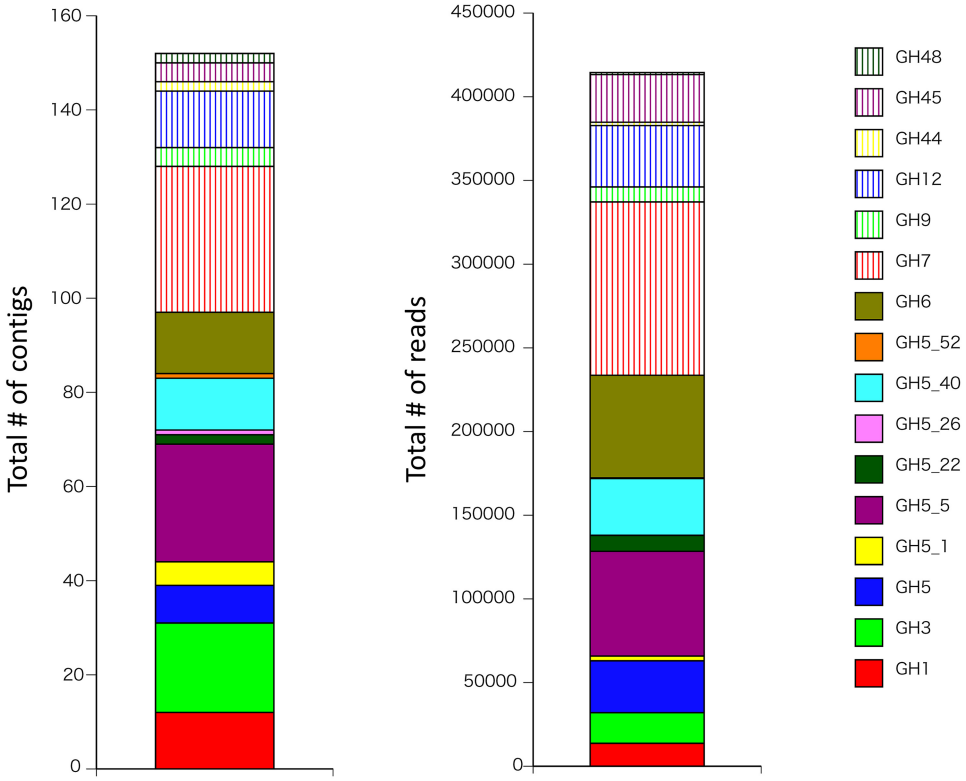

FIG 3 Number of contigs and reads assigned to glycoside hydrolase families known to include cellulases.

60S ribosomal proteins, actin, and glyceraldehyde-3-phosphate dehydrogenase (Data Set S1). Sixty-seven proteins corresponded to hypothetical proteins, 42 were predicted proteins, and 62 were not assigned by NR BLASTp. On the other hand, 24 proteins were classified by auxiliary activity, and four dye-decolorizing peroxidases (DyP) reviewed in reference 24 were also identified (Table 4). Other CAZymes included 11 carbohydrate esterases and 23 glycoside hydrolases categorized as cellulases and hemicellulases (Table 5). The semiquantitative measures of protein abundance were not correlated with the number of reads, a common observation often related to solubility and cellular targeting (intracellular, extracellular, and membrane bound), protein stability, substrate binding, molecular weight, and/or access to trypsin cleavage sites. Previous studies have shown high numbers of basidiomycetous proteins in forest litter, an observation attributed to relatively high C/N ratios (11, 25).

The enzymatic activities of cellobiohydrolase, β-1,4 glucosidase, α-1,4-glucosidase, β-1,4-*N*-acetylglucosaminidase, β-1,4-xylosidase, β-glucuronidase, L-leucine aminopeptidase, and peroxidase were detected at the three sampling points (Fig. S3). Because no laccase transcripts or proteins could be clearly identified, polyphenol oxidase activity may be due to nonspecific oxidations of the l-3,4-dihydroxyphenylalanine (L-DOPA) substrate (Table S4). However, other multicopper oxidases, including ferroxidase-like enzymes (5217211_1, 2197006_3, and 1400590_1; Data Set S1), may have contributed to the L-DOPA activity.

DISCUSSION

Filamentous fungi play a key role in depolymerizing, degrading, and mineralizing the major components of woody cell walls, including cellulose, hemicellulose, and the recalcitrant lignin. Only a fraction of the species has been isolated in pure culture. Moreover, the laboratory conditions employed with model white rot and brown rot fungi fail to mimic natural decay processes. To identify key enzymes and further understand lignocellulose deconstruction, we have examined the metatranscriptome

TABLE 3 Contigs predicted to encode glycoside hydrolases ordered by sequence reads[a]

Contig	No. of reads	Length (bp)	CAZy family[b]	Putative function	E value[c]	Similarity mean (%)[d]	Comment[e]
3240852_1	42,911	1,551	GH7	Cellobiohydrolase 1	0	78.6	SS, MS
6091156_1	25,158	1,281	GH6	Cellobiohydrolase 2	2.21E−98	59.3	SS, MS
4924579_1	24,747	1,587	GH13	1,4-α-Glucan-branching enzyme	0	88.8	
94066_1	24,422	1,169	GH5	Endo-β-1,4-glucanase	1.91E−134	69.5	SS
4034495_1	23,449	1,472	GH45	Endo-β-1,4-glucanase	2.51E−32	56.9	SS
4921502_1	19,419	1,252	GH5_5	Endo-β-1,4-glucanase	8.65E−160	83	SS, MS
5743057_1	18,678	845	GH12	Endo-β 1,4-glucanase	2.54E−115	77.9	SS, MS
4739131_4	17,714	1,657	GH5	Glycoside hydrolase	2.11E−74	54.9	SS
1384861_1	16,216	1,295	GH6	Cellobiohydrolase 2	1.57E−88	58.1	SS, MS
6836211_1	15,440	1,335	GH18	Chitinase	1.49E−62	64.2	
3859657_1	14,542	1,457	GH114	Endo-α-1,4 polygalactosaminidase	8.40E−90	69.5	
3529359_1	14,380	1,570	GH16	β-1,3-Glucanase	1.72E−109	68.5	SS
3589366_1	13,195	1,464	GH7	Cellobiohydrolase 1	0	78.5	SS, MS
3098980_1	13,193	1,072	GH16	Endo-1,3-β-glucanase	2.52E−106	70.4	
2908735_1	10,927	1,113	GH79	Glycoside hydrolase	1.82E−74	68.1	
3561636_2	9,572	1,222	GH10	Endo-1,4-β xylanase	9.07E−158	69.7	SS
65078_1	9,266	1,125	GH7	Cellobiohydrolase 1	1.99E−144	75.9	CBM1
5394650_1	8,876	1,568	GH5_22	Glycoside hydrolase	1.36E−81	66	
1142146_1	8,843	1,125	GH5_5	Endo-β-1,4-glucanase	1.97E−151	76.8	
4728183_1	8,453	1,939	GH128	Glycoside hydrolase	1.89E−125	70.9	SS
98832_1	7,998	943	GH128	Glycoside hydrolase	5.62E−88	65.9	
2374420_1	7,848	1,075	GH9	Glycoside hydrolase	3.18E−50	52.2	
2989759_1	7,548	1,266	GH128	Glycoside hydrolase	1.48E−50	52.2	
247968_1	7,473	1,442	GH5_40	Glycoside hydrolase	2.96E−70	58.1	CBM8
4884037_2	7,291	965	GH53	Endo-1,4-β-galactanase	2.92E−151	76.6	
5204286_1	6,982	1,044	GH128	Glycoside hydrolase	3.96E−103	66.8	
830359_1	6,946	1,312	GH1	β-Glucosidase	1.70E−140	68.5	
3175817_1	6,832	1,625	GH5_7	Endo-1,4-β-mannanase	0	80.1	SS, MS
2132535_1	6,435	1,193	GH105	Glycoside hydrolase	4.62E−107	66.9	
1970615_2	5,800	1,048	GH7	Cellobiohydrolase 1	1.47E−134	76.5	MS

[a]Complete information, including BLASTx analyses, InterPro, and Gene Ontology designations, as well as mass spectrometry results, are listed in Data Set S1 in the supplemental material.
[b]CAZy families were identified by dbCAN (Yin et al. [56]).
[c]E value of top BLASTx hit.
[d]Average sequence similarity to the top 10 BLASTx hits.
[e]SS, SignalP-determined secretion signal; MS, LC-MS/MS-identified proteins; CBM1, carbohydrate-binding module family 1.

and metaproteome of extensively decayed lodgepole pine. In aggregate, the results support complex enzymatic interactions carried out by diverse microbial communities.

The majority of the classified sequences were most closely related to Basidiomycota, followed by cellulolytic Ascomycota, slime molds, and other Protista. Species-level taxonomic assignments are likely biased by the skewed representation of genomes available in the NCBI databases. This is particularly problematic when discriminating brown rot and white rot fungi (15), unless certain white rot-specific genes are detected, such as the MnPs (Table 2; see also Table S1 in the supplemental material). In aggregate, our results strongly suggest that white and brown rot fungi are simultaneously active in decaying lodgepole pine (Fig. 5; see also Fig. S3). Our analysis cannot resolve fine spatial relationships between fungi, and their interactions (e.g., mutualistic, antagonistic, and neutral) remain uncertain. However, the findings are consistent with the coexistence of white and brown rot fungi following laboratory inoculation of spruce logs and placement in forest settings (3, 5, 26). More recently, internal transcribed spacer 2 (ITS2) analyses of Norway spruce (*Picea abies*) logs in unmanaged stands identified various basidiomycetes, including several white and brown rot species (27). Mäkipää et al. reported that most species were rare and that the top 30 accounted for 50% of all operational taxonomic units (OTUs) (27). Our BLASTp counts suggest similar levels of species richness, with the top 30 hits accounting for 43% (18,952) of the contigs. However, we did not observe abundant mycorrhizal species (27), and our results surely underestimate species diversity because of the dependency on physiological activity as well as the lability of RNA targets. These results stand in contrast

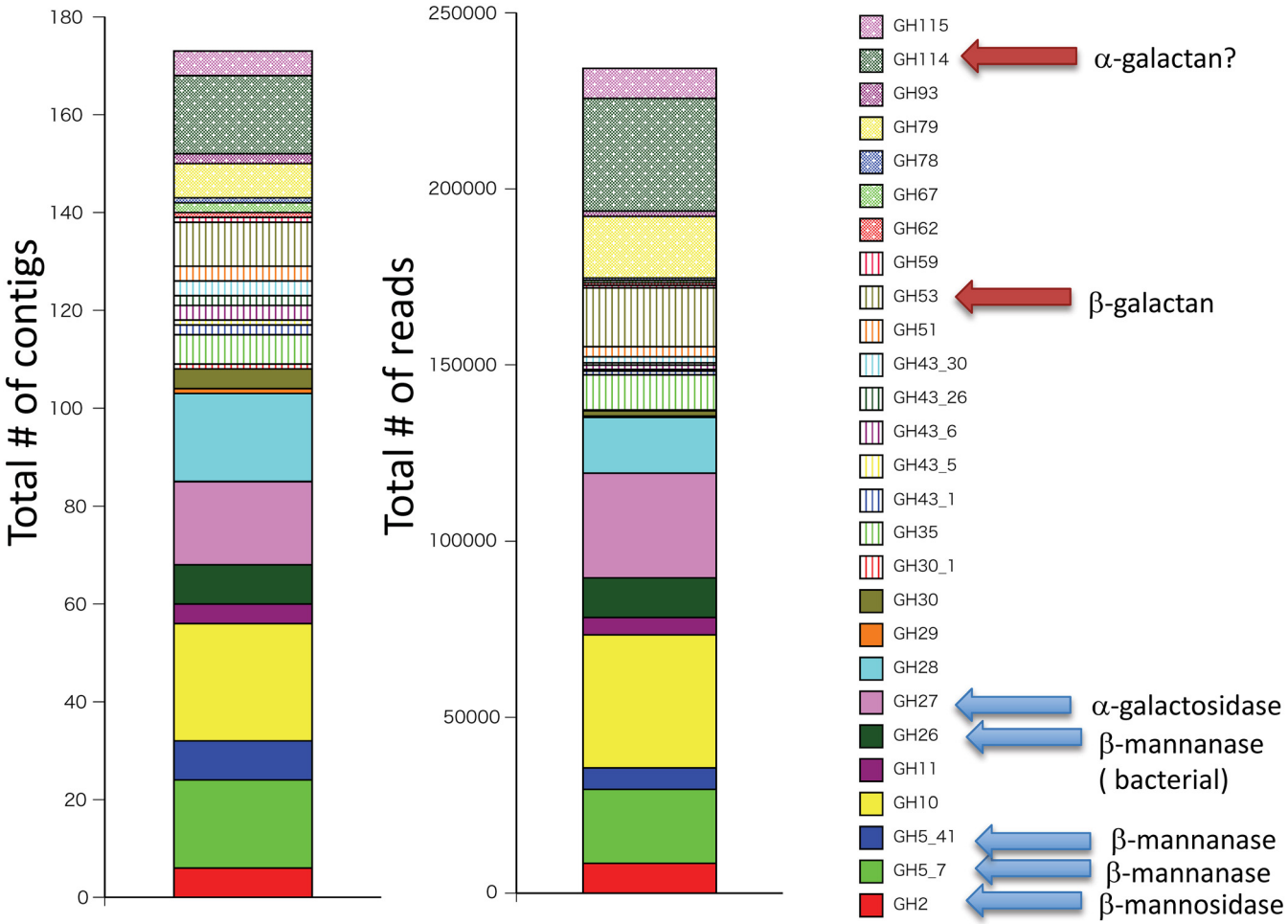

FIG 4 Number of contigs and reads assigned to glycoside hydrolase families known to include hemicellulases.

to metatranscriptome investigations of *Pinus taeda*, where few mycorrhizal species are active (28). In this context, we recognize that the observed patterns would be quite different on other wood species under wet and/or cool conditions. Our sampling was confined to *P. contorta* during a dry period in early summer and, although sampling was not designed to invite statistically valid comparisons, there seemed relatively little difference in the fire-disturbed versus undisturbed samples (Table S2 and Fig. S1 and S2).

Unexpectedly, the second most common top BLAST hits were *Phialocephala* spp. (Fig. 5; see also Fig. S2 in the supplemental material). A well-established endophyte of conifer needles, *P. scopiformis*, produces the anti-insectan compound rugulosin and confers increased tolerance to spruce budworm. The root endophyte *Phialocephala subalpina* (29, 30) is closely related to *P. scopiformis* and, together, these species constitute 5.8% (2,542) of the total number of top hits. Possibly, an undescribed *Phialocephala* sp. or variant strain encodes the observed transcripts and peptides. The genomes of *P. scopiformis* (31) and *P. subalpina* feature numerous CAZymes and, in view of the expression patterns reported here, it seems probable that filamentous basidiomycetes and ascomycetous *Phialocephala* spp. participate in the late stages of *P. contorta* decay.

Our analyses identified an array of genes directly and indirectly involved in lignocellulose degradation. Eighteen MnP-encoding contigs were present (Data Set S1), and peptides matching eight of these were detected (Data Set S1). Generally considered ligninolytic enzymes, amino acid alignments were 53% to 67% identical to that of

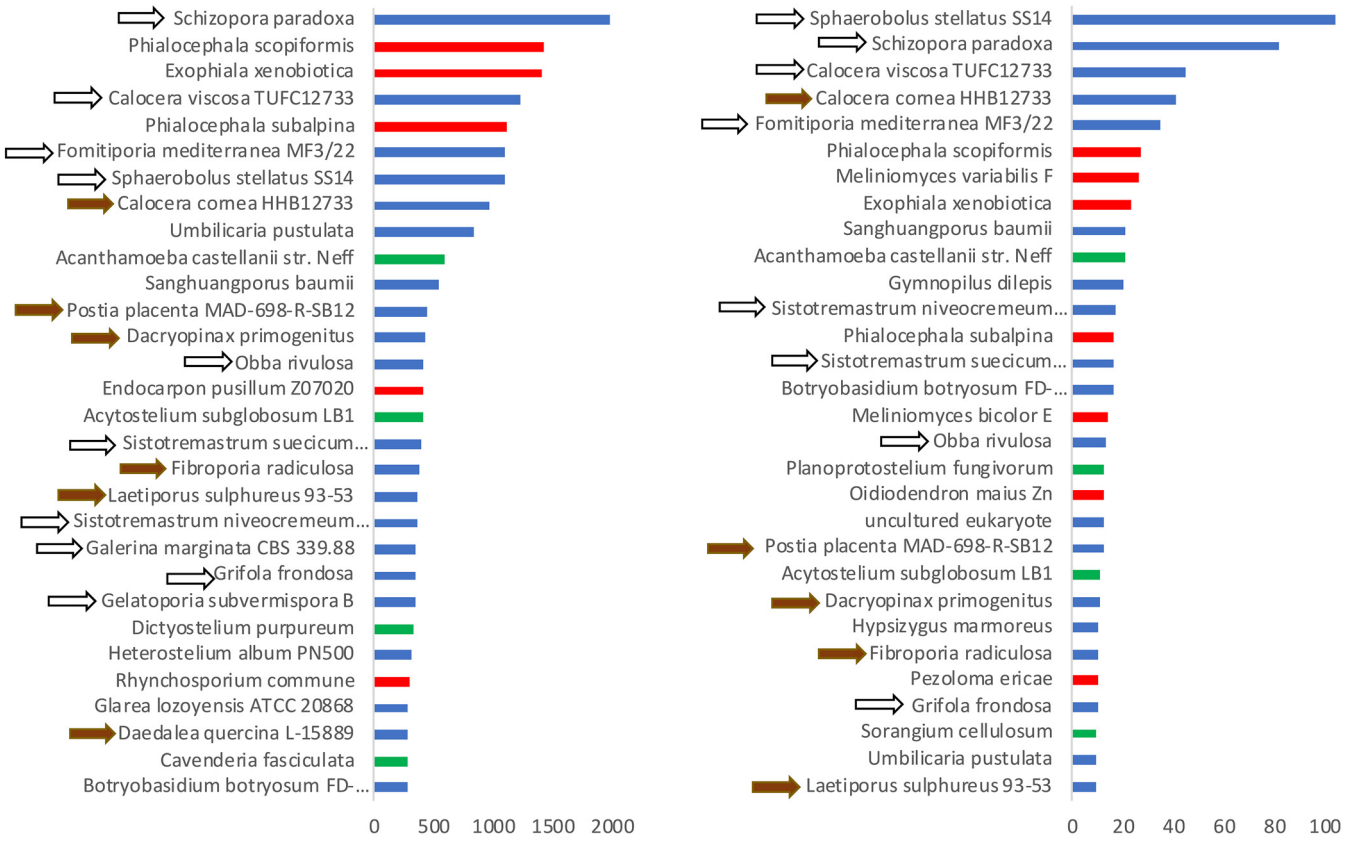

FIG 5 Distributions of top 30 BLASTp (NR database) hits among translations of all 52,011 contigs (left) and for 1,316 contigs (right) identified as CAZyme encoding. The 30 species account for 43% and 54% of the total top hits for all proteins and the CAZyme subset, respectively. White and brown arrows indicate decay type, where known. Fill colors correspond to Basidiomycota (blue), Ascomycota (red), and various other eukaryotes or bacteria (green).

Phanerochaete chrysosporium MnP1 (UniProt accession Q02567) and, within aligned regions, key residues involved in Mn binding and catalysis were conserved (32). In contrast to MnPs, which are widely distributed among white rot fungi (12, 33), lignin peroxidases and versatile peroxidases were not detected. We also observed an array of alcohol oxidases (AA3_3s) that may play a role in supplying extracellular H_2O_2 to the peroxidases. The roles of six DyP peroxidases, three heme-thiolate peroxidases (HTPs), and six chloroperoxidases in ligninolysis, if any, remain unclear (34). The transcripts and activities of these enzymes have been reported in forest litter (35) and, although lacking the oxidative potential to attack lignin, they may be involved in the oxidation and hydroxylation of aromatic metabolites derived from lignin (34). The peptides corresponding to four Dyp genes were identified, but none were detected for the chloroperoxidases and HTPs. Neither transcripts nor peptides were identified for laccases, suggesting no significant role in ligninolysis, at least in the late stages of wood decay.

Other redox enzymes assigned to AA families provide additional insight into degradative mechanisms. We were unable to detect LPMO peptides by MS/MS, but the genes (AA9) were particularly numerous and the transcripts abundant, with 65 contigs and 93,889 transcripts (Table 2 and Fig. 2; see also Data Set S1 in the supplemental material). Assuming that these Cu-dependent enzymes are secreted, they likely play an important role in cellulose cleavage, especially the 12 genes that feature a CBM1 domain (Data Set S1). They may also oxidize xyloglucan and glucomannans, as recently demonstrated for an LPMO from the brown rot fungus *Gloeophyllum trabeum* (36). Interestingly, LPMO activity was recently shown to be dependent on H_2O_2 (37). This may partly explain the number (26), high transcript levels (60,929 reads), and peptide spectrum matches (PSMs) of putative alcohol oxidases (Tables 2 and 5; see also Fig. S1). These family AA3 enzymes generate peroxide from various substrates, including meth-

TABLE 4 Glycoside hydrolases identified in decayed *Pinus contorta* by mass spectrometry

Contig and frame	No. of reads	Length (bp)	CAZy family	E value[a]	Coverage (%)	No. of peptides	No. of PSMs	No. of unique peptides	Sequest HT score
4346763_2_5	1,289	974	GH1	1.77E−123	12	3	5	3	13
4346763_4_2	134	980	GH1	5.00E−117	12	3	5	3	13
4346763_3_1	708	993	GH1	8.16E−121	9	2	3	2	8
4459897_1_1	260	884	GH10	1.63E−72	15	3	7	3	20
3889902_1_4	3,745	1,235	GH10	1.18E−172	7	2	5	2	17
2058669_1_6	2,552	1,145	GH10	8.35E−98	8	2	2	2	7
3960173_1_1	602	936	GH12	2.08E−142	6	2	4	2	12
3166842_1_5	1,268	1,146	GH17	1.92E−145	14	3	5	3	15
2491547_1_6	1,188	1,068	GH3	8.07E−91	13	2	5	2	5
3730185_1_5	1,252	831	GH47	8.13E−166	8	2	3	2	8
6091156_1_3	25,158	1,281	GH6	2.70E−100	23	5	24	4	73
1553595_1_2	2,108	926	GH6	5.22E−156	11	2	7	2	24
1384861_1_6	16,216	1,295	GH6	1.13E−102	8	2	4	1	8
1384861_2_1	4,220	1,303	GH6	2.48E−103	5	2	3	1	7
658106_4_6	1,932	1,273	GH7	1.72E−137	17	5	24	4	74
658106_7_2	1,550	1,024	GH7	1.50E−97	16	4	23	3	70
3240852_1_4	42,911	1,551	GH7	0	20	7	23	6	63
4852_1_6	697	764	GH7	3.56E−70	11	2	12	1	34
3223568_3_6	477	871	GH7	6.16E−115	10	2	9	1	26
3240852_2_6	1,163	965	GH7	1.59E−104	16	3	9	3	26
1970615_2_6	5,800	1,048	GH7	2.18E−142	18	4	5	3	13
3589366_2_3	1,295	1,109	GH7	4.77E−168	14	3	3	2	5
3589366_1_6	13,195	1,464	GH7	0	6	2	2	1	4

[a]BLASTp NR.

anol. Both white rot and brown rot fungi demethylate lignin and, in the case of *Gloeophyllum trabeum* brown rot, evidence suggests that methanol oxidase contributes peroxide to advance the Fenton reaction (19).

The mechanism(s) of brown rot decay remain unsettled. Recent genome annotations make it clear that cellobiose dehydrogenase is not essential, as this multifunctional enzyme is absent from the genomes of several efficient brown rot fungi. Our analysis also failed to identify the transcript in decayed lodgepole pine. On the other hand, the data are consistent with hydroxyl radicals generated via benzoquinone reductase and oxalate-Fe^{3+} chelates (20–22). Specifically, we identified 25 putative benzoquinone reductases (32,831 reads), 20 oxalate decarboxylases (28,450 reads), and an oxalate transporter which together might modulate hydroxyl radical production (38) (Data Set S1). In contrast, our inability to detect any laccase transcripts undermines its involvement in the process (39–41).

Without doubt, lodgepole pine decay involves the combined activities of functionally diverse enzymes and fungal species. The synergistic activities of conventional endo- and exocellobiohydrolases are well known. More recently, LPMO has been shown to boost the performance of these hydrolases (42, 43). Although our study selected for eukaryotic mRNA, genes most closely related to bacteria were occasionally identified. Several studies have implicated bacteria as part of complex consortia involved in wood decay (44–47, and reviewed in reference 48). We also found genes most closely related to slime molds and other protists, as well as several bacteria, many of which have been associated with decomposition. The enzymatic machinery and interactions among these species merit further investigation.

MATERIALS AND METHODS

Sample description and RNA preparation. Loose and crumbling material from the upper surface of three extensively decayed lodgepole pine logs was collected in western Montana in July 2014. The logs were in direct contact with the ground. No clear zones of fungal colonization or fruiting bodies were observed on the decayed wood or in the immediate vicinity. However, portions of the decayed surfaces had dark cubicle regions interspersed with lighter-colored fibrous areas, often associated with brown rot and white rot, respectively (Fig. S5). Locations included U.S. Forest Service's Tenderfoot Creek Experimental Forest (TCEF) at 46.923333, −110.869444 (46°55′24″N, 110°52′10″W) (altitude, 2,238 m). This specific site was within a mature lodgepole pine stand with a dense canopy, sparse ground cover, and

TABLE 5 Redox enzymes potentially involved in lignocellulose degradation identified in decayed *Pinus contorta* by mass spectrometry

Contig and frame	No. of reads	Length (bp)	Description[a]	CAZy family	E value[b]	Coverage (%)	No. of peptides	No. of PSMs	No. of unique peptides	Sequest HT score
4793784_3_2	4,023	932	Manganese peroxidase	AA2	1.68E−159	7	2	3	1	8
4793784_13_2	2,332	1,097	Manganese peroxidase	AA2	0	8	2	3	1	9
2280897_3_6	3,374	1,119	Alcohol oxidase	AA3_3	0	26	8	23	8	66
2280897_9_1	1,468	1,170	Alcohol oxidase	AA3_3	0	20	6	11	5	34
798557_1_1	7,736	1,563	Alcohol oxidase	AA3_3	0	15	5	10	2	27
798557_5_2	3,018	1,095	Alcohol oxidase	AA3_3	0	17	4	8	1	20
798557_13_6	1,908	1,337	Alcohol oxidase	AA3_3	0	11	3	6	1	15
798557_17_6	2,693	1,051	Alcohol oxidase	AA3_3	2.12E−166	18	3	6	1	16
2280897_7_2	3,087	1,095	Alcohol oxidase	AA3_3	1.83E−177	11	2	5	1	15
2280897_11_6	1,698	1,169	Alcohol oxidase	AA3_3	0	9	3	3	2	9
798557_25_4	176	899	Alcohol oxidase	AA3_3	7.64E−157	13	2	5	0	12
536886_1_6	4,574	1,455	Alcohol oxidase	AA3_3	0	9	3	7	3	22
2766776_1_4	910	784	Benzoquinone reductase	AA6	7.36E−98	12	2	2	2	6
3005685_1_6	258	810	Benzoquinone reductase	AA6	6.80E−87	10	2	12	1	34
1341126_2_3	1,595	1,039	Benzoquinone reductase	AA6	7.50E−120	26	6	26	5	76
1507360_1_3	9,562	1,007	Benzoquinone reductase	AA6	1.28E−109	21	5	19	4	56
1507360_2_6	263	993	Benzoquinone reductase	AA6	2.95E−70	12	3	14	2	39
3719648_4_6	986	1,106	Benzoquinone reductase	AA6	6.41E−111	27	8	43	7	123
1712785_3_2	1,051	816	Benzoquinone reductase	AA6	8.34E−112	28	5	34	4	99
1712785_2_4	739	948	Benzoquinone reductase	AA6	5.49E−144	20	5	24	4	71
3711757_1_4	925	885	NADH-quinone OR	AA6	1.86E−106	7	2	10	1	27
3834150_1_3	5,521	862	Benzoquinone reductase	AA6	9.20E−111	8	2	10	2	30
3719648_1_3	1,059	828	NADH-quinone OR	AA6	5.06E−82	12	3	11	2	29
4644641_1_2	2,872	842	Dyp-type peroxidase		3.56E−93	37	8	37	6	109
4644641_2_5	1,109	863	Dyp-type peroxidase		4.33E−79	33	5	32	3	85
3735866_1_2	448	873	Dyp-type peroxidase		6.27E−45	20	3	17	2	51
3427787_2_2	1,036	1,107	Dyp-type peroxidase		1.96E−81	28	6	9	5	29

[a]OR, oxidoreductase.
[b]BLASTp NR.

no history of fire in over 140 years. Two samples were collected near Gibbon's Pass on the Bitterroot National Forest, MT. The area was the site of a catastrophic fire in 2001 and, at the time of collection, featured a dense stand of lodgepole saplings. Considerable ground cover was predominantly *Xerophyllum tenax*, *Lupinus sericeus*, and *Vaccinium scoparium*. The GP1 log was in a relatively flat area at 45.754444, −113.909444 (45°45′16″N, 113°54′34″W) (altitude, 2,146 m), whereas the GP2 log was located on an incline at 45.755278, −113.910556 (45°45′19″N, 113°54′38″W) (altitude, 2,138 m). The length of time during which the trees were down could not be determined, although at the time of fall, cellulose, hemicellulose, and lignin levels are estimated to be 44%, 31%, and 27%, respectively (49). All samples were ground with an electric-blade coffee grinder, passed through a 2-mm sieve, shipped overnight on ice, and stored at −80°C.

Approximately 1 g of the ground samples was extracted with the Mo Bio RNA isolation kit (catalog no. 12866-25; Carlsbad, CA), according to the manufacturer's recommendations. The final total-RNA pellet was suspended in 100 μl water. Oligo(dT)$_{25}$ DynaBeads (Oslo, Norway) was prepared as suggested by the manufacturer. Seventy microliters of the beads was washed and suspended in 100 μl of binding buffer (20 mM Tris-HCl [pH 7.5], 1.0 M LiCl, 2 mM EDTA). To eliminate secondary structure, RNA was incubated at 65°C for 2 min and immediately placed on ice. The RNA and bead solution were mixed and, after occasional inverting over a 5-min period, placed in a Dynal magnet stand. The beads were washed and recaptured twice and the poly(A) RNA eluted with 10 μl water. The poly(A) RNA was incubated at 70°C for 10 min and amplified following the MessageAmp II protocol (Invitrogen, Thermo Fisher Scientific). The anti-sense RNA (aRNA) quantity and quality were assessed using a Qubit fluorometer (Thermo Fisher Scientific) and a 2100 Bioanalyzer (Agilent), respectively.

RNA-seq libraries were prepared and sequenced by the U.S. Department of Energy Joint Genome Institute (Walnut Creek, CA). mRNA was fragmented and reversed transcribed using random hexamers and SSII (Invitrogen), followed by second-strand synthesis. The fragmented cDNA was treated with end-pair, A-tailing, adapter ligation, and eight cycles of PCR. Quantitative PCR (qPCR) was used to determine the concentrations of the libraries. The prepared libraries were quantified using Kapa Biosystems' next-generation sequencing library qPCR kit and run on a Roche LightCycler 480 real-time PCR instrument. The quantified libraries were then prepared for sequencing on the Illumina HiSeq sequencing platform utilizing a TruSeq paired-end cluster kit, v4, and Illumina's cBot instrument to generate a clustered flow cell for sequencing. Sequencing of the flow cell was performed on the Illumina HiSeq-1TB sequencer using HiSeq TruSeq SBS sequencing kits, v4, following a 2 by 150 indexed run recipe. The three sample files were combined, without normalization, for final assembly. DNASTAR's SeqMan NGen (version 14.1) was used to perform *de novo* transcriptome assemblies with default parameters (mer size, 21; clustering match, 97%), with a minimum of 101 sequences per contig (average,

590). The resulting assemblies were sorted according to the number of reads and length with SeqMan Pro. Those contigs exceeding 750 bp were initially BLASTx queried against the RefSeq protein database, and EMBL-EBI was used to predict InterPro domains as well as transmembrane helices, secretion signals, and enzyme codes. The top BLASTx hits were used to guide protein translations of 39,765 genes and, for the 12,246 contigs lacking significant similarity, the longest ORFs among six strands were translated. For BLASTp searches of NR, contigs were translated based on BLASTx results or, in the case of little or no significant sequence homology, the longest ORFs were used. Transeq 5.0.0 was used to translate ORFs within all contigs in all frames for the mass spectrometry database (below) (50, 51). Gene Ontology annotations were determined using Blast2GO.

Protein extraction and mass spectrometry identification. Total soluble protein was extracted from approximately 5 g Wiley ground wood samples using the NoviPure soil protein extraction kit (catalog no. 30000-20; Mo Bio, Qiagen, Carlsbad, CA). Nanoliquid chromatography-MS/MS (nanoLC-MS/MS) was used to identify proteins, as described previously (52–54).

Crude protein extracts were further purified with trichloroacetic acid (TCA) precipitation, followed by multiple acetone washes. The pellets were resolubilized to a concentration of ~1 mg/ml of dry weight-liquid with 8 M urea and aliquots taken for protein concentration determination (Pierce 660 nm protein assay kit; Thermo Fisher Scientific). Twenty-five micrograms of urea solubilized protein extract was 10× concentrated with liquid-liquid extraction (methanol-chloroform-water), trypsin/LysC digested, and OMIX C_{18} SPE cleaned up (Agilent Technologies); finally, 1.5 μg was loaded for nanoLC-MS/MS analysis using an 1100 Nanoflow system (Agilent Technologies) connected to a hybrid linear ion trap-Orbitrap mass spectrometer (LTQ-Orbitrap Elite; Thermo Fisher Scientific) equipped with an EASY-Spray electrospray source. Chromatography of peptides prior to mass spectral analysis was accomplished using capillary emitter column (PepMap C_{18} column, 3 μM, 100 Å, 150 by 0.075 mm; Thermo Fisher Scientific), onto which 2 μl of purified peptides was automatically loaded. The nano-high-performance liquid chromatography (nanoHPLC) system delivered solvents A (0.1% [vol/vol] formic acid) and B (99.9% [vol/vol] acetonitrile, 0.1% [vol/vol]) formic acid) at 0.50 μl/min to load the peptides (over a 30-min period) and 0.3 μl/min to elute peptides directly into the nano-electrospray; a gradual gradient from 3% (vol/vol) B to 20% (vol/vol) B over 154 min was used and concluded with a 12-min fast gradient from 20% (vol/vol) B to 50% (vol/vol) B, at which time a 5-min flash-out from 50 to 95% (vol/vol) B took place. As peptides eluted from the HPLC-column/electrospray source survey MS scans were acquired in the Orbitrap, with a resolution of 120,000, followed by MS/MS fragmentation of 20 most intense peptides detected in the precursor MS1 scan from *m/z* 380 to 1,800; redundancy was limited by dynamic exclusion. Raw data files were imported into Thermo Proteome Discoverer (PD version 2.2.0.388) for database searching and assignment of identification significance. A user-defined metagenomic database was compiled from 6 frame translations of 52,011 assembled contigs (>750 bp), generating 312,066 protein entries. The Sequest HT search engine (within PD) assigned peptide and protein identifications within a 1% false-discovery rate using 15 ppm mass tolerance for peptide and 0.6 Da for a fragment ion mass. Variable methionine oxidation with asparagine and glutamine deamidation plus fixed cysteine carbamidomethylation was specified. Further stringency for an acceptable identification was applied by requiring at least two peptides per individual protein and an Xcorr value of 1.8 or greater per individual peptide spectrum match.

It should be noted that under the conditions employed, mass spectrometry detection of extracellular proteins is subject to false-negative results due to the frequency of trypsin cleavage, low molecular weight, substrate binding, and/or proteolytic degradation. False-positive results, in contrast, are unlikely.

The potential activities of 10 extracellular wood-degrading enzymes were quantified on a limited amount of ground sample (<40 mg [dry weight]) from each location, as follows: cellobiohydrolase (CBH; an exocellulase), β-glucosidase (BG; which hydrolyzes cellobiose into glucose), α-glucosidase (AG; which hydrolyzes starch), β-xylosidase (BX; which degrades the xylose component of hemicellulose), β-glucuronidase (BGLU; which degrades the β-glucuronic acid component of hemicellulose), β-*N*-acetyl-glucosaminidase (NAG; which breaks down chitin), acid phosphatase (AP; which releases inorganic phosphate from organic matter), leucine-aminopeptidase (LAP; which breaks down polypeptides), polyphenol oxidase (PPO; which oxidizes phenols), and peroxidase (PER; including oxidases that degrade lignin). Samples were stored frozen at −80°C after collection and analyzed as described previously (55), with the following modification: to ensure detectable activity, the LAP assay was conducted in 0.2 M phosphate buffer (pH 6.8), with 1 mM fluorogenic substrate. All enzyme activities were calculated as nanomoles activity per gram per hour and ln-transformed prior to interpretation.

Data availability. Fastq files were deposited in the Sequence Read Archive under biosample accession numbers SAMN07573382 (GP1), SAMN07573383 (TCEF), and SAMN07573384 (GP2). The raw mass spectrometry data were deposited to the Chorus repository (https://chorusproject.org; no. 1478) for public sharing and visualization.

SUPPLEMENTAL MATERIAL

Supplemental material for this article may be found at https://doi.org/10.1128/AEM.01133-18.

SUPPLEMENTAL FILE 1, XLSX file, 18.7 MB.

SUPPLEMENTAL FILE 2, PDF file, 2.2 MB.

ACKNOWLEDGMENTS

The work conducted by the U.S. Department of Energy Joint Genome Institute, a DOE Office of Science User Facility supported by the Office of Science of the U.S. Department of Energy under contract DE-AC02-05CH11231. Research was also supported by NSF grants 1457695 and 1457721 to J.M.B. and D.C., respectively, and by JSPS Grant-in-Aid for Scientific Research 16K18727 to C.H. The research in the Martin Lab was funded by the French National Research Agency through the project SYMWOOD (Laboratory of Excellence Advanced Research on the Biology of Tree and Forest Ecosystems, grant ANR-11-LABX 0002 01).

We thank Forest Service staff Robin Taylor-Davenport for identifying ground cover vegetation and Helen Smith for collecting samples at the Tenderfoot Creek Experimental Forest.

REFERENCES

1. Ottosson E, Norden J, Dahlberg A, Edman M, Jonsson M, Larsson KH, Olsson J, Penttila R, Stenlid J, Ovaskainen O. 2014. Species associations during the succession of wood-inhabiting fungal communities. Fungal Ecol 11:17–28. https://doi.org/10.1016/j.funeco.2014.03.003.
2. Arnstadt T, Hoppe B, Kahl T, Kellner H, Kruger D, Bauhus J, Hofrichter M. 2016. Dynamics of fungal community composition, decomposition and resulting deadwood properties in logs of *Fagus sylvatica*, *Picea abies* and *Pinus sylvestris*. Forest Ecol Manage 382:129–142. https://doi.org/10.1016/j.foreco.2016.10.004.
3. Lindner DL, Vasaitis R, Kubartova A, Allmer J, Johannesson H, Banik MT, Stenlid J. 2011. Initial fungal colonizer affects mass loss and fungal community development in *Picea abies* logs 6 yr after inoculation. Fungal Ecol 4:449–460. https://doi.org/10.1016/j.funeco.2011.07.001.
4. Rajala T, Tuomivirta T, Pennanen T, Mäkipää R. 2015. Habitat models of wood-inhabiting fungi along a decay gradient of Norway spruce logs. Fungal Ecol 18:48–55. https://doi.org/10.1016/j.funeco.2015.08.007.
5. Rajala T, Peltoniemi M, Hantula J, Mäkipää R, Pennanen T. 2011. RNA reveals a succession of active fungi during decay of Norway spruce logs. Fungal Ecol 4:437–448. https://doi.org/10.1016/j.funeco.2011.05.005.
6. Větrovský T, Stursova M, Baldrian P. 2016. Fungal communities in soils: soil organic matter degradation. Methods Mol Biol 1399:89–100. https://doi.org/10.1007/978-1-4939-3369-3_5.
7. Damon C, Lehembre F, Oger-Desfeux C, Luis P, Ranger J, Fraissinet-Tachet L, Marmeisse R. 2012. Metatranscriptomics reveals the diversity of genes expressed by eukaryotes in forest soils. PLoS One 7:e28967. https://doi.org/10.1371/journal.pone.0028967.
8. Žifčáková L, Vetrovsky T, Howe A, Baldrian P. 2016. Microbial activity in forest soil reflects the changes in ecosystem properties between summer and winter. Environ Microbiol 18:288–301. https://doi.org/10.1111/1462-2920.13026.
9. Hesse CN, Mueller RC, Vuyisich M, Gallegos-Graves LV, Gleasner CD, Zak DR, Kuske CR. 2015. Forest floor community metatranscriptomes identify fungal and bacterial responses to N deposition in two maple forests. Front Microbiol 6:337. https://doi.org/10.3389/fmicb.2015.00337.
10. Keiblinger KM, Fuchs S, Zechmeister-Boltenstern S, Riedel K. 2016. Soil and leaf litter metaproteomics—a brief guideline from sampling to understanding. FEMS Microbiol Ecol 92:fiw180. https://doi.org/10.1093/femsec/fiw180.
11. Bastida F, Torres IF, Moreno JL, Baldrian P, Ondono S, Ruiz-Navarro A, Hernandez T, Richnow HH, Starke R, Garcia C, Jehmlich N. 2016. The active microbial diversity drives ecosystem multifunctionality and is physiologically related to carbon availability in Mediterranean semi-arid soils. Mol Ecol 25:4660–4673. https://doi.org/10.1111/mec.13783.
12. Cullen D. 2014. Wood decay, p 41–62. *In* Martin F (ed), Ecological genomics of fungi. Wiley-Blackwell, New York, NY.
13. Hatakka A, Hammel KE. 2010. Fungal biodegradation of lignocelluloses. *In* Hofrichter M (ed), Industrial applications, 2nd ed, vol 10. Springer-Verlag, Berlin, Germany.
14. Lombard V, Golaconda Ramulu H, Drula E, Coutinho PM, Henrissat B. 2014. The carbohydrate-active enzymes database (CAZy) in 2013. Nucleic Acids Res 42:D490–D495. https://doi.org/10.1093/nar/gkt1178.
15. Riley R, Salamov AA, Brown DW, Nagy LG, Floudas D, Held BW, Levasseur A, Lombard V, Morin E, Otillar R, Lindquist EA, Sun H, LaButti KM, Schmutz J, Jabbour D, Luo H, Baker SE, Pisabarro AG, Walton JD, Blanchette RA, Henrissat B, Martin F, Cullen D, Hibbett DS, Grigoriev IV. 2014. Extensive sampling of basidiomycete genomes demonstrates inadequacy of the white-rot/brown-rot paradigm for wood decay fungi. Proc Natl Acad Sci U S A 111:9923–9928. https://doi.org/10.1073/pnas.1400592111.
16. Floudas D, Binder M, Riley R, Barry K, Blanchette RA, Henrissat B, Martinez AT, Otillar R, Spatafora JW, Yadav JS, Aerts A, Benoit I, Boyd A, Carlson A, Copeland A, Coutinho PM, de Vries RP, Ferreira P, Findley K, Foster B, Gaskell J, Glotzer D, Gorecki P, Heitman J, Hesse C, Hori C, Igarashi K, Jurgens JA, Kallen N, Kersten P, Kohler A, Kues U, Kumar TK, Kuo A, LaButti K, Larrondo LF, Lindquist E, Ling A, Lombard V, Lucas S, Lundell T, Martin R, McLaughlin DJ, Morgenstern I, Morin E, Murat C, Nagy LG, Nolan M, Ohm RA, Patyshakuliyeva A, et al. 2012. The Paleozoic origin of enzymatic lignin decomposition reconstructed from 31 fungal genomes. Science 336:1715–1719. https://doi.org/10.1126/science.1221748.
17. Plett JM, Kemppainen M, Kale SD, Kohler A, Legue V, Brun A, Tyler BM, Pardo AG, Martin F. 2011. A secreted effector protein of *Laccaria bicolor* is required for symbiosis development. Curr Biol 21:1197–1203. https://doi.org/10.1016/j.cub.2011.05.033.
18. Levasseur A, Drula E, Lombard V, Coutinho PM, Henrissat B. 2013. Expansion of the enzymatic repertoire of the CAZy database to integrate auxiliary redox enzymes. Biotechnol Biofuels 6:41. https://doi.org/10.1186/1754-6834-6-41.
19. Daniel G, Volc J, Filonova L, Plihal O, Kubatova E, Halada P. 2007. Characteristics of *Gloeophyllum trabeum* alcohol oxidase, an extracellular source of H_2O_2 in brown rot decay of wood. Appl Environ Microbiol 73:6241–6253. https://doi.org/10.1128/AEM.00977-07.
20. Shimokawa T, Nakamura M, Hayashi N, Ishihara M. 2004. Production of 2,5-dimethoxyhydroquinone by the brown-rot fungus *Serpula lacrymans* to drive extracellular Fenton reaction. Holzforschung 58:305–310. https://doi.org/10.1515/HF.2004.047.
21. Suzuki MR, Hunt CG, Houtman CJ, Dalebroux ZD, Hammel KE. 2006. Fungal hydroquinones contribute to brown rot of wood. Environ Microbiol 8:2214–2223. https://doi.org/10.1111/j.1462-2920.2006.01160.x.
22. Varela E, Tien M. 2003. Effect of pH and oxalate on hydroquinone-derived hydroxyl radical formation during brown rot wood degradation. Appl Environ Microbiol 69:6025–6031. https://doi.org/10.1128/AEM.69.10.6025-6031.2003.
23. Meier KK, Jones SM, Kaper T, Hansson H, Koetsier MJ, Karkehabadi S, Solomon EI, Sandgren M, Kelemen B. 2018. Oxygen activation by Cu LPMOs in recalcitrant carbohydrate polysaccharide conversion to monomer sugars. Chem Rev 118:2593–2635. https://doi.org/10.1021/acs.chemrev.7b00421.
24. Linde D, Ruiz-Duenas FJ, Fernandez-Fueyo E, Guallar V, Hammel KE, Pogni R, Martinez AT. 2015. Basidiomycete DyPs: genomic diversity, structural-functional aspects, reaction mechanism and environmental significance. Arch Biochem Biophys 574:66–74. https://doi.org/10.1016/j.abb.2015.01.018.
25. Schneider T, Keiblinger KM, Schmid E, Sterflinger-Gleixner K, Ellersdorfer G, Roschitzki B, Richter A, Eberl L, Zechmeister-Boltenstern S, Riedel K. 2012. Who is who in litter decomposition? Metaproteomics reveals major microbial players and their biogeochemical functions. ISME J 6:1749–1762. https://doi.org/10.1038/ismej.2012.11.
26. Kubartová A, Ottosson E, Stenlid J. 2015. Linking fungal communities to

wood density loss after 12 years of log decay. FEMS Microbiol Ecol 91:fiv032. https://doi.org/10.1093/femsec/fiv032.
27. Mäkipää R, Rajala T, Schigel D, Rinne KT, Pennanen T, Abrego N, Ovaskainen O. 2017. Interactions between soil- and dead wood-inhabiting fungal communities during the decay of Norway spruce logs. ISME J 11:1964–1974. https://doi.org/10.1038/ismej.2017.57.
28. Liao HL, Chen Y, Bruns TD, Peay KG, Taylor JW, Branco S, Talbot JM, Vilgalys R. 2014. Metatranscriptomic analysis of ectomycorrhizal roots reveal genes associated with *Piloderma-Pinus* symbiosis: improved methodologies for assessing gene expression in situ. Environ Microbiol 16:3730–3742. https://doi.org/10.1111/1462-2920.12619.
29. Robicheau BM, Young AP, LaButti K, Grigoriev IV, Walker AK. 2017. The complete mitochondrial genome of the conifer needle endophyte, *Phialocephala scopiformis* DAOMC 229536 confirms evolutionary division within the fungal *Phialocephala fortinii* s.l.–*Acephala appalanata* species complex. Fungal Biol 121:212–221. https://doi.org/10.1016/j.funbio.2016.11.007.
30. Schlegel M, Munsterkotter M, Guldener U, Bruggmann R, Duo A, Hainaut M, Henrissat B, Sieber CM, Hoffmeister D, Grunig CR. 2016. Globally distributed root endophyte *Phialocephala subalpina* links pathogenic and saprophytic lifestyles. BMC Genomics 17:1015. https://doi.org/10.1186/s12864-016-3369-8.
31. Walker AK, Frasz SL, Seifert KA, Miller JD, Mondo SJ, LaButti K, Lipzen A, Dockter RB, Kennedy MC, Grigoriev IV, Spatafora JW. 2016. Full genome of *Phialocephala scopiformis* DAOMC 229536, a fungal endophyte of spruce producing the potent anti-insectan compound rugulosin. Genome Announc 4:e01768-15. https://doi.org/10.1128/genomeA.01768-15.
32. Martínez AT. 2002. Molecular biology and structure-function of lignin-degrading heme peroxidases. Enzyme Microb Technol 30:425–444. https://doi.org/10.1016/S0141-0229(01)00521-X.
33. Janusz G, Pawlik A, Sulej J, Swiderska-Burek U, Jarosz-Wilkolazka A, Paszczynski A. 2017. Lignin degradation: microorganisms, enzymes involved, genomes analysis and evolution. FEMS Microbiol Rev 41:941–962. https://doi.org/10.1093/femsre/fux049.
34. Hofrichter M, Ullrich R, Pecyna MJ, Liers C, Lundell T. 2010. New and classic families of secreted fungal heme peroxidases. Appl Microbiol Biotechnol 87:871–897. https://doi.org/10.1007/s00253-010-2633-0.
35. Kellner H, Luis P, Pecyna MJ, Barbi F, Kapturska D, Kruger D, Zak DR, Marmeisse R, Vandenbol M, Hofrichter M. 2014. Widespread occurrence of expressed fungal secretory peroxidases in forest soils. PLoS One 9:e95557. https://doi.org/10.1371/journal.pone.0095557.
36. Kojima Y, Varnai A, Ishida T, Sunagawa N, Petrovic DM, Igarashi K, Jellison J, Goodell B, Alfredsen G, Westereng B, Eijsink VG, Yoshida M. 2016. A lytic polysaccharide monooxygenase with broad xyloglucan specificity from the brown-rot fungus *Gloeophyllum trabeum* and its action on cellulose-xyloglucan complexes. Appl Environ Microbiol 82:6557–6572. https://doi.org/10.1128/AEM.01768-16.
37. Bissaro B, Rohr AK, Muller G, Chylenski P, Skaugen M, Forsberg Z, Horn SJ, Vaaje-Kolstad G, Eijsink VGH. 2017. Oxidative cleavage of polysaccharides by monocopper enzymes depends on H_2O_2. Nat Chem Biol 13:1123–1128. https://doi.org/10.1038/nchembio.2470.
38. Presley GN, Zhang J, Schilling JS. 2016. A genomics-informed study of oxalate and cellulase regulation by brown rot wood-degrading fungi. Fungal Genet Biol 112:64–70. https://doi.org/10.1016/j.fgb.2016.08.004.
39. Kaneko S, Yoshitake K, Itakura S, Tanaka H, Enoki A. 2005. Relationship between production of hydroxyl radicals and degradation of wood, crystalline cellulose, and lignin-related compound or accumulation of oxalic acid in cultures of brown-rot fungi. J Wood Sci 51:262–269. https://doi.org/10.1007/s10086-004-0641-3.
40. Jensen KA, Jr, Houtman CJ, Ryan ZC, Hammel KE. 2001. Pathways for extracellular Fenton chemistry in the brown rot basidiomycete *Gloeophyllum trabeum*. Appl Environ Microbiol 67:2705–2711. https://doi.org/10.1128/AEM.67.6.2705-2711.2001.
41. Wei D, Houtman CJ, Kapich AN, Hunt CG, Cullen D, Hammel KE. 2009. Laccase and its role in production of extracellular reactive oxygen species during wood decay by the brown rot basidiomycete *Postia placenta*. Appl Environ Microbiol 76:2091–2097. https://doi.org/10.1128/AEM.02929-09.
42. Vaaje-Kolstad G, Westereng B, Horn SJ, Liu Z, Zhai H, Sorlie M, Eijsink VG. 2010. An oxidative enzyme boosting the enzymatic conversion of recalcitrant polysaccharides. Science 330:219–222. https://doi.org/10.1126/science.1192231.
43. Song B, Li B, Wang X, Shen W, Park S, Collings C, Feng A, Smith SJ, Walton JD, Ding SY. 2018. Real-time imaging reveals that lytic polysaccharide monooxygenase promotes cellulase activity by increasing cellulose accessibility. Biotechnol Biofuels 11:41. https://doi.org/10.1186/s13068-018-1023-1.
44. Kubartová A, Ottosson E, Dahlberg A, Stenlid J. 2012. Patterns of fungal communities among and within decaying logs, revealed by 454 sequencing. Mol Ecol 21:4514–4532. https://doi.org/10.1111/j.1365-294X.2012.05723.x.
45. Rajala T, Peltoniemi M, Pennanen T, Mäkipää R. 2012. Fungal community dynamics in relation to substrate quality of decaying Norway spruce (*Picea abies* [L.] Karst.) logs in boreal forests. FEMS Microbiol Ecol 81:494–505. https://doi.org/10.1111/j.1574-6941.2012.01376.x.
46. Hoppe B, Krger K, Kahl T, Arnstadt T, Buscot F, Bauhus J, Wubet T. 2015. A pyrosequencing insight into sprawling bacterial diversity and community dynamics in decaying deadwood logs of *Fagus sylvatica* and *Picea abies*. Sci Rep 5:9456. https://doi.org/10.1038/srep09456.
47. Valásková V, de Boer W, Gunnewiek PJ, Pospisek M, Baldrian P. 2009. Phylogenetic composition and properties of bacteria coexisting with the fungus *Hypholoma fasciculare* in decaying wood. ISME J 3:1218–1221. https://doi.org/10.1038/ismej.2009.64.
48. Johnston SR, Boddy L, Weightman AJ. 2016. Bacteria in decomposing wood and their interactions with wood-decay fungi. FEMS Microbiol Ecol 92:fiw179. https://doi.org/10.1093/femsec/fiw179.
49. Lieu PJ, Kelsey RG, Shafizadeh F. 1979. Some chemical characteristics of green and dead lodgepole pine and western white pine. Service UF, Intermountain Forest and Range Experiment Station, Ogden, UT.
50. Rice P, Longden I, Bleasby A. 2000. EMBOSS: the European Molecular Biology Open Software Suite. Trends Genet 16:276–277. https://doi.org/10.1016/S0168-9525(00)02024-2.
51. Blankenberg D, Taylor J, Schenck I, He J, Zhang Y, Ghent M, Veeraraghavan N, Albert I, Miller W, Makova KD, Hardison RC, Nekrutenko A. 2007. A framework for collaborative analysis of ENCODE data: making large-scale analyses biologist-friendly. Genome Res 17:960–964. https://doi.org/10.1101/gr.5578007.
52. Hori C, Ishida T, Igarashi K, Samejima M, Suzuki H, Master E, Ferreira P, Ruiz-Duenas FJ, Held B, Canessa P, Larrondo LF, Schmoll M, Druzhinina IS, Kubicek CP, Gaskell JA, Kersten P, St. John F, Glasner J, Sabat G, Splinter BonDurant S, Syed K, Yadav J, Mgbeahuruike AC, Kovalchuk A, Asiegbu FO, Lackner G, Hoffmeister D, Rencoret J, Gutierrez A, Sun H, Lindquist E, Barry K, Riley R, Grigoriev IV, Henrissat B, Kues U, Berka RM, Martinez AT, Covert SF, Blanchette RA, Cullen D. 2014. Analysis of the *Phlebiopsis gigantea* genome, transcriptome and secretome provides insight into its pioneer colonization strategies of wood. PLoS Genet 10:e1004759. https://doi.org/10.1371/journal.pgen.1004759.
53. Fernandez-Fueyo E, Ruiz-Duenas FJ, Ferreira P, Floudas D, Hibbett DS, Canessa P, Larrondo LF, James TY, Seelenfreund D, Lobos S, Polanco R, Tello M, Honda Y, Watanabe T, Ryu JS, Kubicek CP, Schmoll M, Gaskell J, Hammel KE, St. John FJ, Vanden Wymelenberg A, Sabat G, Splinter BonDurant S, Syed K, Yadav JS, Doddapaneni H, Subramanian V, Lavin JL, Oguiza JA, Perez G, Pisabarro AG, Ramirez L, Santoyo F, Master E, Coutinho PM, Henrissat B, Lombard V, Magnuson JK, Kues U, Hori C, Igarashi K, Samejima M, Held BW, Barry KW, LaButti KM, Lapidus A, Lindquist EA, Lucas SM, Riley R, Salamov AA, et al. 2012. Comparative genomics of *Ceriporiopsis subvermispora* and *Phanerochaete chrysosporium* provide insight into selective ligninolysis. Proc Natl Acad Sci U S A 109:5458–5463. https://doi.org/10.1073/pnas.1119912109.
54. Ryu JS, Shary S, Houtman CJ, Panisko EA, Korripally P, St. John FJ, Crooks C, Siika-Aho M, Magnuson JK, Hammel KE. 2011. Proteomic and functional analysis of the cellulase system expressed by *Postia placenta* during brown rot of solid wood. Appl Environ Microbiol 77:7933–7941. https://doi.org/10.1128/AEM.05496-11.
55. Talbot JM, Martin VJ, Kohler A, Henrissat B, Peay KG. 2015. Functional guild classification predicts the enzymatic role of fungi in litter and soil biogeochemistry. Soil Biol Biochem 88:441–456. https://doi.org/10.1016/j.soilbio.2015.05.006.
56. Yin Y, Mao X, Yang J, Chen X, Mao F, Xu Y. 2012. dbCAN: a web resource for automated carbohydrate-active enzyme annotation. Nucleic Acids Res 40:W445–W451. https://doi.org/10.1093/nar/gks479.